JOURNAL OF VIROLOGY, May 2005, p. 6281–6290 Vol. 79, No. 10
0022-538X/05/$08.00+0 doi:10.1128/JVI.79.10.6281–6290.2005

Genetic Determinants of Cell Type-Specific Poliovirus Propagation in HEK 293 Cells

Stephanie A. Campbell, Jennifer Lin, Elena Y. Dobrikova, and Matthias Gromeier*

Department of Molecular Genetics and Microbiology, Duke University Medical Center, Durham, North Carolina 27710

Received 6 April 2004/Accepted 27 December 2004

The ability of poliovirus to propagate in neuronal cells can be reduced by introducing appropriate nucleotide substitutions into the viral genome. Specific mutations scattered throughout the poliovirus genome yielded the live attenuated vaccine strains of poliovirus. Neuron-specific propagation deficits of the Sabin strains are partially encrypted within a confined region of the internal ribosomal entry site (IRES), which carries attenuating point mutations in all three serotypes. Recently, high levels of neurovirulence attenuation were achieved with genetically engineered polioviruses containing heterologous IRES elements. This is exemplified with poliovirus recombinants replicating under control of a human rhinovirus type 2 (HRV2) IRES element. We have carried out experiments delineating the genetic basis for neuronal IRES function. Neuronal dysfunction of the HRV2 IRES is determined mainly by IRES stem-loop domain V, the locus for attenuating point mutations within the Sabin strains. Neuronal incompetence associated with HRV2 IRES domain V is substantially more pronounced than that observed with the attenuating IRES point mutation of the Sabin serotype 1 vaccine strain. Mix-and-match recombination of polio and HRV2 IRES domain V suggests that the attenuation phenotype correlates with overall structural features rather than primary sequence. Our experiments have identified HEK 293 cells as a novel system for the study of neuron-specific replication phenotypes of poliovirus. This cell line, originally derived from embryonic human kidney, has recently been described to display neuronal characteristics. We report propagation properties in HEK 293 cells for poliovirus recombinants with attenuated neurovirulence in experimental animals that corroborate this observation.

Poliovirus (PV), a positive-strand RNA virus of approximately 7,500 nucleotides (nt), is the prototypic member of the genus *Enterovirus* in the family *Picornaviridae*. PV is the causative agent of poliomyelitis, a paralytic condition complicating ~1% of all PV infections. The incidence of poliomyelitis has been drastically reduced since the introduction of two effective vaccines—the live attenuated (Sabin) strains and the formalin-inactivated (Salk) vaccine. Serial passage of wild-type (wt) PV in various culture systems yielded the serotype 1 and 3 Sabin strains, while serotype 2 is a naturally occurring variant with inherently reduced neurovirulence (48).

It is generally assumed that the excellent safety record of the Sabin strains (the rate of vaccine-associated paralytic poliomyelitis [VAPP] is estimated at 0.14 per 1,000,000 doses) (60) is a direct reflection of tissue type-specific deficiencies that affect their propagation in the human central nervous system (CNS). Nevertheless, despite over 40 years of successful application, the molecular basis for neuroattenuation of the Sabin strains is not completely understood (16).

Elucidation of the genomic sequences of PV type 1 (Sabin) [PV1(S)] (38) and PV3(S) (53, 58) and comparison to their wt progenitors PV type 1 (Mahoney) [PV1(M)] (30, 56) and PV type 3 (Leon) (52, 56) have revealed the genetic basis of the attenuation phenotype. However, assigning genetic markers in the Sabin strains responsible for attenuated growth in the primate CNS has been far more difficult than anticipated (reviewed in reference 61). Genetic analyses of neuroattenuation have focused on two areas of the PV genome that harbor mutations in all of the Sabin strains—the internal ribosomal entry site (IRES) and the coding region for the capsid proteins (reviewed in reference 40). In addition, the coding region for the viral RNA-dependent RNA polymerase $3D^{pol}$ of PV1(S) has also been implicated (see reference 41 and references therein).

All Sabin serotypes feature point mutations within a confined region of IRES stem-loop domain (SLD) V (see Fig. 2 and 4) that have been implicated in the attenuation phenotype. The IRES occupies the uncommonly large 5′ untranslated regions (UTR) of all picornaviruses and mediates 5′-end independent translation initiation of the uncapped viral genome (27, 42). Evidence for involvement of IRES SLD V in neuroattenuation stems from studies of PV3(S)-associated VAPP, revealing reversion of the IRES mutation at nt 472 to the wt sequence (C→U) (13). Accordingly, PV3(S) strains with the wt (Leon) IRES sequence displayed enhanced neurovirulence in nonhuman primates (59). Similarly, reversion of IRES SLD V mutations at nt 480 (G→A) of PV1(S) and nt 481 (G→A) of PV2(S) occurred in patients with VAPP (20), with corresponding effects on neurovirulence in nonhuman primates (29, 34).

SLD V mutations were proposed to influence neurovirulence through their effect on IRES secondary structure (21, 35, 51). This is underscored by the isolation of PV1(S) revertants with increased neurovirulence that acquired a transition at nt 525 (U→C), restoring the stem structure disrupted by the attenuating nt 480 (G) mutation (8). Furthermore, neuronal IRES activity may be affected by higher-order structures involving SLDs V and VI (18, 22). Secondary structure conformation associated with PV3(S) nt 472 (C) has been associated

* Corresponding author. Mailing address: Dept. of Molecular Genetics and Microbiology, Duke University Medical Center, Box 3020, Durham, NC 27710. Phone: (919) 668-6205. Fax: (919) 684-8735. E-mail: grome001@mc.duke.edu.

with reduced translation activity in vitro (21, 55) and may reflect altered affinity for IRES *trans*-acting factors (39, 42).

We previously constructed PV1(RIPO), a chimeric virus where the cognate PV IRES is replaced with its counterpart from human rhinovirus type 2 (HRV2) (19). PV1(RIPO) grows with wt kinetics in HeLa and malignant glioma cells (17) but is severely attenuated for growth in neuron-like cell lines commonly used to assess PV attenuation phenotypes (1, 32), e.g., Sk-N-Mc neuroblastoma cells (19). Growth deficiency in neuron-like cells correlates with elimination of pathogenicity in mice transgenic for the poliovirus receptor CD155 (19) and in nonhuman primates (18).

Here we report fine mapping of the genetic basis for neuroattenuation associated with the HRV2 IRES through analysis of truncated IRES elements and their gene expression profiles in neuron-like cells. With a minor contribution by SLD VI, neuronal HRV2 IRES incompetence strongly correlates with SLD V sequences and their potential effect on secondary structure. Analyses of IRES-driven reporter gene expression in HeLa and neuron-like cells suggest that cell type-specific propagation of PV1(RIPO) cannot be explained by translation efficiency at the IRES alone.

HEK 293 cells, human embryonic kidney cells transformed with sheared adenovirus type 5 DNA (15), were recently reported to exhibit neuronal characteristics suggesting preferential transformation of neuroblastic precursors in human embryonic kidney (50). Our findings strongly corroborate these observations and establish HEK 293 cells as a tissue culture model superior to neuroblastoma cell lines for the evaluation of PV neurovirulent phenotypes.

Our observations point toward a common molecular mechanism for neuronal deficiencies of HRV2 and Sabin IRES elements, although neuronal dysfunction mediated by HRV2 IRES SLD V is substantially more pronounced than that produced by nt 480 (G) of PV1(S). Furthermore, the neuronal incompetence associated with HRV2 IRES SLD V is significantly more stable than that of PV1(S) upon serial passage in HEK 293 cells. Enhanced attenuation of neurovirulence and improved genetic stability of this phenotype may indicate a comparatively favorable biological safety profile of live attenuated vaccines based on PV/HRV chimeras.

MATERIALS AND METHODS

Construction of PV/HRV2 IRES chimeras. All viruses with recombinant IRESes were based on an EcoRI-SacI cloning cassette described previously for the construction of PV1(RIPO) (19). The genetic structure of the cloning cassette is as follows: PV1(M) cloverleaf, EcoRI-SacI insert site for recombinant IRESes, PV1(S) P1 (coding region for the structural gene products), and PV1(M) P2-P3 and 3′ UTR-poly(A).

Construction of EcoRI-SacI inserts for PV1/M(IRES) and PV1/S(IRES) was achieved through PCR amplification of PV1(M) IRES domains II-VI with primers 1 (5′-CCCGGAATTCAGACGCACAAAACCAAG-3′) and 2 (5′-CTGAG CTCCCATTATGATACAATTGTCTGATT-3′) from corresponding cDNA templates. Inserts for the deletion variants PV1/M(δ6) and PV1/S(δ6) were generated with primers 1 and 3 (5′-GCGAGCTCCCATGGTCAGCCACAAT AAAATAAAAG-3′). PCR amplification of HRV2 IRES domains II-VI from HRV2 genomic cDNA to generate the insert for RPS was accomplished with primers 4 (5′-GGGAATTCACTTAGAAGTTTTTCA-3′) and 5 (5′-CTGAGC TCCCATGGTGCCAATATATATATTGT-3′). Deletion of HRV2 IRES SLD VI for the EcoRI-SacI insert of RPS(δ6) was achieved with PCR amplification of an IRES fragment from HRV2 genomic cDNA using primers 4 and 6 (5′-GCG AGCTCCCATGGTCAAATATAAAGGAGAAAGTG-3′). In each case, the appropriate EcoRI-SacI fragment was ligated into the EcoRI-SacI cloning cassette.

Substitution of HRV2 IRES SLD V with its counterpart from PV1(M) to yield RPS(δ6-PV5) was accomplished by PCR amplification of a fragment encompassing HRV2 IRES SLD II to IV using primers 1 and 7 (5′-GGAGGATCCAAA GCGAGCACACGGG-3′) and a fragment encompassing PV1(M) SLD V amplified with primers 8 (5′-CCGGATCCTCCGGCCCCTGAATGCG-3′) and 3. Both fragments were ligated into the EcoRI-SacI cloning cassette.

For the generation of RPS(δ6-PV5a), an HRV2 IRES fragment encompassing SLDs II-IV and including a minor portion of PV1(M) SLD V was PCR amplified with primers 4 and 9 (5′-GTCTGCAGGGTTAAGGTTAG-3′). The distal loop region of PV1(M) SLD V was PCR amplified using primers 10 (5′-GTCTGCA GCAGGTGGTCACAAAC-3′) and 11 (5′-GTCAATTGCGCGTTACGACAG G-3′). The remaining portion of domain V including the descending stem was PCR generated using an HRV2 cDNA as a template with primers 12 (5′-GTC AATTGCGGGATGGGAC-3′) and 6. The three fragments were ligated with the EcoRI-SacI cloning cassette to yield RPS(δ6-PV5a).

To produce RPS(δ6-PV5b), annealed complementary 5′-phosphorylated oligonucleotides (5′-GCTAGTGGTCACAAACCAGTGATTGGCTAGTCGTA ATGAC-3′ and 5′-AATTGCTCATTACGACTAGCCAATCACTGGTTTGTG ACCACTAGCTGCA-3′) were ligated to a vector obtained by digesting RPS(δ6-PV5a) with PstI and MunI. RPS(δ6-PV5c) was generated similarly using annealed complementary oligonucleotides (5′-GCTAGAGGTCACAAACCAG TGATTATCTAGTCGTAATGAGC-3′ and 5′-AATTGCTCATTACGACTAG ATAATCACTGGTTTGTGACCTCTAGCTGCA-3′).

To rederive virus of each construct, plasmid cDNA was linearized through digestion with AviII and used as a template for T7 RNA polymerase-mediated in vitro transcription. The resulting viral RNA transcripts were transfected into HeLa cells to produce infectious viral particles.

Cells, infections, and one-step growth curves. HeLa R19, Sk-N-Mc (ATCC, Manassas, VA), and HEK 293 (National Cancer Institute, Bethesda, MD) cells were propagated in Dulbecco's modified Eagle medium (DMEM) (Invitrogen, Carlsbad, CA) supplemented with 10% (vol/vol) fetal bovine serum (FBS), penicillin/streptomycin/amphotericin B, and fungizone. Cells were maintained at 37°C in 5% CO_2. To determine viral replication kinetics, tissue culture monolayers were overlaid with DMEM containing virus at a multiplicity of infection of 10. Subsequently, plates were rocked for 30 min at room temperature (rt). Cells were then washed three times with serum-free DMEM to remove unbound virus particles and covered with DMEM supplemented with 2% FBS. Infected cells were incubated at 37°C and at various times postinfection (p.i.) were lysed by two freeze/thaw cycles. Viral titers were quantified by plaque assay on HeLa cells as described before (19).

For serial passaging, subconfluent HEK 293 cell monolayers in 6-cm dishes were infected with virus at a multiplicity of infection of 10 in a volume of 500 μl serum-free DMEM. The cells were rocked for 30 min and subsequently overlaid with 1.5 ml DMEM–2% FBS. Plates were incubated at 37°C until cytopathic effects were observed; in the absence of cytopathic effects, incubation was for 24 h. Infected cells were then lysed by two cycles of freezing and thawing. Cell lysate (500 μl) was applied to a fresh HEK 293 cell monolayer to start the next passage.

Analysis of IRES sequence after passaging. Total cellular RNA was isolated from infected cell lysates with TRIzol reagent (Invitrogen) and served as a template for reverse transcription using standard procedures and PV-specific primer 13 (5′-CATGTGCGCCCACTTTCTGTG-3′). The cDNA was employed as a template in a PCR with primers 13 and 14 (5′-CGCCTGTTTTATACTCC CTTCCC-3′), and the resulting PCR product (spanning a portion of the 5′ cloverleaf, the entire IRES region, and a fragment of the coding region for the capsid proteins) was sequenced.

Western blot analyses. Lysates from DMS79 (kindly provided by J. Keene, Duke University), HEK 293, HeLa, Vero (kindly provided by K. Chumakov, Food and Drug Administration), Sk-N-Mc, and SH SY5Y (both ATCC) cells for neural marker expression analysis were prepared as follows. Cell monolayers in 250-ml flasks were washed three times with phosphate-buffered saline (PBS) and subsequently scraped into 4 ml PBS. DMS79 grow in suspension and were used directly. Cell suspensions were centrifuged to pellet the cells, which were suspended in 2 volumes of lysis buffer (100 mM KCl, 25 mM EDTA, 5 mM MgCl2, 10 mM HEPES, 0.5% Nonidet P-40, protease inhibitor cocktail [Roche, Indianapolis, IN]; pH 7.0). Next, the resuspended cells underwent two freeze/thaw cycles to promote cell lysis. Total protein levels of the resulting lysates were quantified by Bradford assay, and equal quantities were loaded onto 4 to 12% Bis-Tris NuPAGE gels (Invitrogen) or Novex 4% Tris-Glycine gels (Invitrogen) for sodium dodecyl sulfate-polyacrylamide gel electrophoresis (SDS-PAGE).

To prepare cell lysates of virus-infected cells for the analysis of viral protein

synthesis, HeLa, Sk-N-Mc, or HEK 293 monolayers on 35-mm dishes were washed with PBS and cells were lysed in SDS-PAGE loading buffer at various intervals p.i. as previously described (9). Samples from these whole cell lysates were resolved by SDS-PAGE on 4 to 12% Bis-Tris NuPAGE gels.

All SDS-PAGE gels were electrophoretically transferred to nitrocellulose membranes (Schleicher & Schuell, Keene, NH), and blots were blocked with 4% dry milk in Tris-buffered saline (TBS; 100 mM Tris-buffered saline, pH 8.5) overnight. Following blocking, blots were incubated with primary antibody (α-neurofilament [200 kDa], α-nestin, α-neuron-specific enolase, α-neurofilament [145 kDa], α-neurofilament [70 kDa], α-tau, and α-βIII tubulin [Chemicon, Temecula, CA]; α-PV 2BC/2C monoclonal antibody [kindly provided by E. Wimmer, State University of New York at Stony Brook, NY]) at a 1:1,000 dilution in TBST (TBS, 0.05% Tween 20) for 1 h at rt. Subsequently, the blots were treated with biotinylated goat α-mouse or α-rabbit immunoglobulin G (Vector Labs, Burlingame, CA) diluted at 1:500 in TBST for 30 min at rt. Finally, the blots were incubated with streptavidin-peroxidase conjugate (Roche, Indianapolis, IN) at a dilution of 1:2,000 in TBST for 20 min at rt. All blots were developed with the enhanced chemiluminescence substrate system according to the manufacturer's instructions (Amersham, Piscataway, NJ) and exposed to X-ray film.

Luciferase expression assays. To generate luciferase reporter vector pHRV-Luc-PVA50, pUC19 was digested with BamHI and SalI and ligated with three PCR-amplified fragments. These fragments encompassed (i) the T7 promoter and the 5′ terminal portion (nt 1 to 1110) of PV-RIPO (19), (ii) the *Renilla* luciferase (rLuc) coding sequence, and (iii) the PV1(M) 3′ UTR followed by a 50-mer poly(A) tail. PCR fragments i, ii, and iii were amplified with primers 15 (5′-GCGGATCCTAATACGACTCACTATAGGTTAAAAC-3′) and 16 (5′-CTTTCGAAGTTTGCCCAAAGAGTCCCATG-3′); 17 (5′-ACTTCGAAGTTTATGATCCAG-3′) and 18 (5′-GGTCTAGATTGTTCATTTTTGAGAACTCG-3′); and 19 (5′-GGTCTAGAAACCCTACCTCAGTCGAATTG-3′) and 20 (5′-GGGTCGAC[T]$_{50}$CTCCGAA-3′), respectively. pHRV-Luc-PVA50 was digested with EcoRI and SacI, and an EcoRI/SacI-digested PV1(M) fragment encompassing IRES SLDs II-VI was ligated into the vector to yield pPV1(M)-Luc-PVA50. A capped control reporter vector was constructed as follows. The firefly luciferase (fLuc) open reading frame was amplified from plasmid pGL3 (Promega, Madison, WI) by PCR with primers 21 (5′-GCCTCGAGATGGAAGACGCCAAAAACATAAAGAAAGG-3′) and 22 (5′-GCTCTAGATTACACGGCGATCTTTCCGCCCTTCTTG-3′) and ligated into XhoI/XbaI-digested pTNT (Promega). The resulting construct contains the β-globin leader sequence, fLuc, and poly(A) tail.

IRES-driven and cap-driven reporter plasmids were linearized by digestion with SalI and BamHI, respectively, and used as templates for in vitro transcription with T7 RNA polymerase (19). The linearized capped reporter template was supplied with cap structure analog (New England Biolabs, Beverly, MA) during the reaction. In vitro transcripts were treated with TURBO DNase (Ambion, Austin, TX) and purified using the RNeasy cleanup protocol (QIAGEN, Valencia, CA). Tissue culture dishes (35 mm) containing 8×10^5 cells were transfected with 0.05 μg of IRES reporter RNA and 0.05 μg of capped reporter RNA using DMRIE-C transfection reagent (Invitrogen) in OPTI-MEM reduced serum medium (Invitrogen). At 2 h posttransfection, the transfection medium was replaced with antibiotic-free DMEM containing 2% FBS. At various intervals posttransfection, the cells were washed with PBS and lysed with 0.2 ml passive luciferase assay lysis buffer (Promega, Madison, WI). rLuc and fLuc activities were determined in a Berthold luminometer (no. LB9507) following Promega's dual luciferase assay protocol.

RESULTS

HEK 293 cells express neuronal proteins. Recent evidence indicates that the adenovirus-transformed HEK 293 cell line, which was derived from primary human embryonic kidney cultures (15), exhibits neuronal properties (50). This assertion is based on the finding that HEK 293 cells express medium and light neurofilament subunits when tested in immunocytochemical and immunoblotting assays (50). We bolstered these findings by testing HEK 293 cells for expression of these and other characteristic neuronal markers in a more rigorous assay. We conducted Western blot analyses of lysates obtained from HEK 293 and a number of other cell lines to detect all three classes of neurofilaments, nestin, βIII-tubulin, neuron-specific enolase, and tau (Fig. 1). Expression of these factors is commonly assessed to determine a neuron-like phenotype (28, 33).

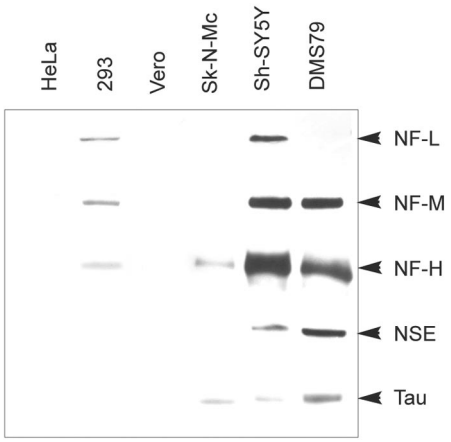

FIG. 1. Expression patterns of neuronal marker proteins in HeLa (human cervical carcinoma), HEK 293 (human embryonic kidney), Vero (African Green Monkey kidney), Sk-N-Mc (human neuroblastoma), Sh-SY5Y (human neuroblastoma), and DMS79 (human small cell lung cancer) cells. Cell extracts were prepared as described in Materials and Methods and utilized for five Western blot analyses of the light (NF-L), medium (NF-M), and heavy (NF-H) neurofilament subunits, neuron-specific enolase (NSE), and tau protein.

Our Western blots revealed that adenovirus-transformed HEK 293 cells express light, medium, and heavy neurofilament subunits (Fig. 1). Sk-N-Mc neuroblastoma cells, a conventional neuronal model cell line used to characterize PV neuron-specific propagation characteristics (9, 19), express detectable levels of only the heavy subunit in our sensitive assay (Fig. 1). Another neuroblastoma cell line, SH-SY5Y, expresses all three neurofilament subunits. The small cell lung carcinoma line DMS79 expresses detectable levels of both the medium and heavy subunits. Furthermore, Sk-N-Mc, SH-SY5Y, and DMS79 express neuron-specific enolase and tau (Fig. 1). No neurofilament expression was detected in HeLa (cervical carcinoma) or Vero (African green monkey kidney) cells (Fig. 1), and we were unable to detect expression of nestin or βIII-tubulin in any of the cell lines tested (data not shown). Our observations indicate that HEK 293 cells express several neuronal markers, corroborating the findings of Shaw et al. (50).

RPS is more attenuated than PV1/S(IRES) in vitro. To test the influence of IRES sequence on replication in neuronal cell lines, we generated PV1 recombinants featuring the IRES elements of PV1(M) [PV1/M(IRES)], PV1(S) [PV1/S(IRES)], or HRV2 [RPS], respectively (Fig. 2A). All virus constructs featuring diverse IRES structures described in this report were based on a PV1(S) derivative (see Materials and Methods). We performed one-step growth curves in HeLa, Sk-N-Mc, and HEK 293 cells to assess the viral growth kinetics corresponding to each IRES element (Fig. 2B). SH-SY5Y frequently did not withstand the infection procedure and therefore was difficult to use in our assays. Since viral growth kinetics in SH-SY5Y cells corresponded to those in Sk-N-Mc cells for all three virus constructs (data not shown), we limited our study to the latter. Additionally, we analyzed the kinetics of viral gene expression by Western blot detection of viral gene products 2BC/2C (Fig. 2C). We consistently observed more-robust gene expression in

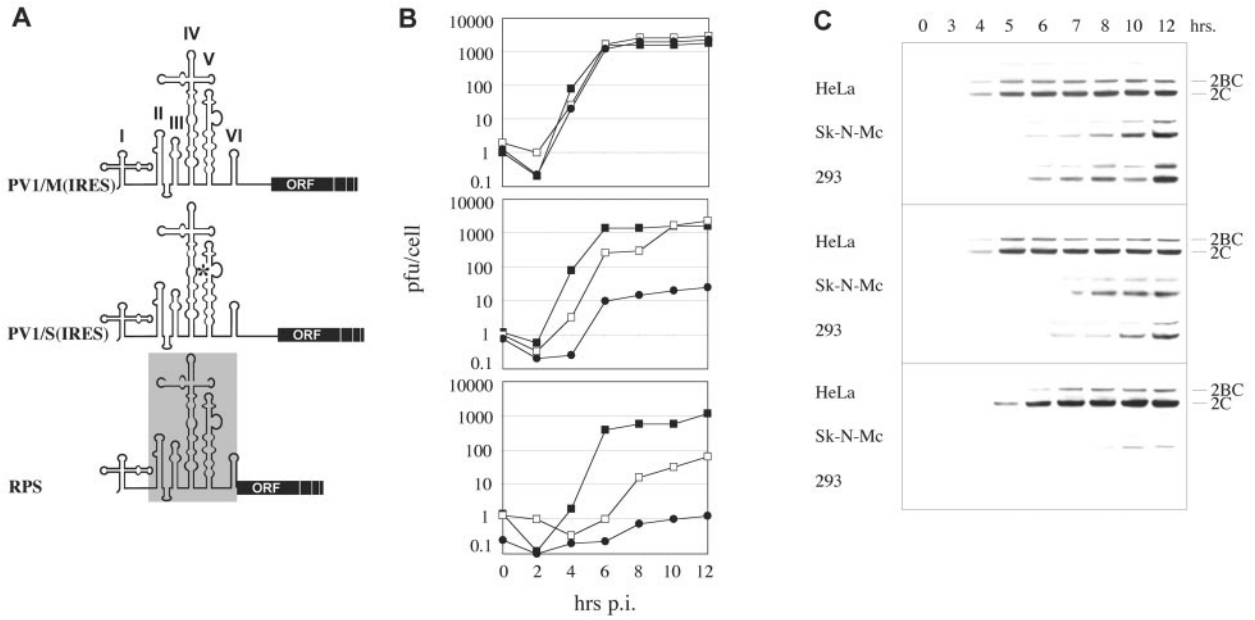

FIG. 2. Genetic structure (A), one-step growth curves (B), and viral gene expression (C) of PV1/M(IRES), PV1/S(IRES), and RPS. (A) The heterologous HRV2 IRES is outlined by a gray box, and the asterisk indicates the approximate position of the attenuating mutation at nt 480 in SLD V of the PV1(S) IRES. Individual 5′ UTR SLDs are indicated by Roman numerals atop. (B) One-step growth kinetics in HeLa (■), Sk-N-Mc (□), and HEK 293 (●) cells were established as described in Materials and Methods. (C) The accumulation of viral gene products was assessed by Western blot detection of the polioviral proteins 2C/2BC at various hours p.i.

HeLa cells compared to HEK 293 and Sk-N-Mc cells, even when viral progeny production was equivalent between cell lines. Based on our observations, we speculate that HeLa cells provide an environment especially conducive to viral gene expression.

Virus propagation and gene expression in HeLa cells were minimally influenced by IRES sequence (Fig. 2). In sharp contrast, cell type-specific propagation levels in neuronal cell lines varied dramatically with IRES identity. Substitution of the Sabin nucleotide at position 480 resulted in slightly decreased growth in neuron-like cells, as PV1/S(IRES) exhibited reduced growth kinetics and viral gene expression in Sk-N-Mc and 293 cells compared to PV1/M(IRES) (Fig. 2B, C). Reduced growth was evident by a prolonged eclipse, delayed accumulation of progeny, and reduced total virus yield 12 h p.i. of HEK 293 cells (Fig. 2B). Interestingly, PV1/S(IRES) grew much more poorly in 293 cells than in Sk-N-Mc cells.

Compared to the moderate deficiencies of PV1/S(IRES), RPS exhibited dramatically diminished propagation in neuronal cell lines (Fig. 2B, C). This was evident in Sk-N-Mc cells, where the total progeny yield 12 h p.i. was <5% of PV1/M(IRES). Surprisingly, there was hardly any progeny production [<0.05% of PV1/M(IRES)] (Fig. 2B) and no detectable viral gene expression 12 h p.i. in HEK 293 cells (Fig. 2C). Despite this severe neuronal growth deficit, RPS growth kinetics mirrored those of PV1/M(IRES) in HeLa cells (Fig. 2B).

Thus, our observations demonstrate that RPS is significantly more impaired than PV1(S) in neuronal cells and that this effect is far more pronounced in HEK 293 cells than in Sk-N-Mc cells. This observation, along with our results implicating HEK 293 cells as neuron-like, prompted us to employ 293 cells exclusively as our neuronal tissue culture model in further studies. To take advantage of this improved tissue culture model for neuronal growth phenotypes of PV, we performed experiments to delineate the genetic basis for neuronal IRES function.

PV IRES SLD V is sufficient for virus growth in neuronal cells. The genetic locus for HRV2 IRES neuronal dysfunction is roughly assigned to the 3′ terminal SLDs V and VI (18). To decipher the genetic basis for neuronal IRES function in greater detail and separate contributions by diverse SLDs, we took advantage of engineered IRES deletion variants. Deletion of SLD VI from type 1 IRESes has been shown to yield viable viruses with reduced neurovirulence (14, 26, 31, 43). In our constructs a highly conserved cryptic AUG codon upstream of the authentic initiating codon was placed into optimal Kozak context to allow translation in the absence of SLD VI (10, 12) (Fig. 3A). Deletion of IRES SLD VI yields a viable virus with slightly reduced viral replication and gene expression in HeLa cells (10, 12). We constructed PV1/M(δ6), PV1/S(δ6), and RPS(δ6) based on the parents PV1/M(IRES), PV1/S(IRES), and RPS (Fig. 3A). As expected, propagation of these viruses in universally permissive HeLa cells was protracted vis-à-vis their parent viruses (compare Fig. 3B and 2B). SLD VI deletion caused a slight cell type-specific growth defect of PV1/M(δ6) in HEK 293 cells that was not observed with the corresponding full-length IRES (compare Fig. 2B and 3B), corroborating a contributing role of this structure in neuronal IRES function (18). Propagation and gene expression of PV1/S(δ6) and RPS(δ6) in HEK 293 cells remained poor, and the IRES-dependent cell type-specific growth pattern was similar to that of parent viruses with full-length IRES structures. These results permitted fine-mapping of genetic determinants of neuronal IRES function within IRES SLD V alone.

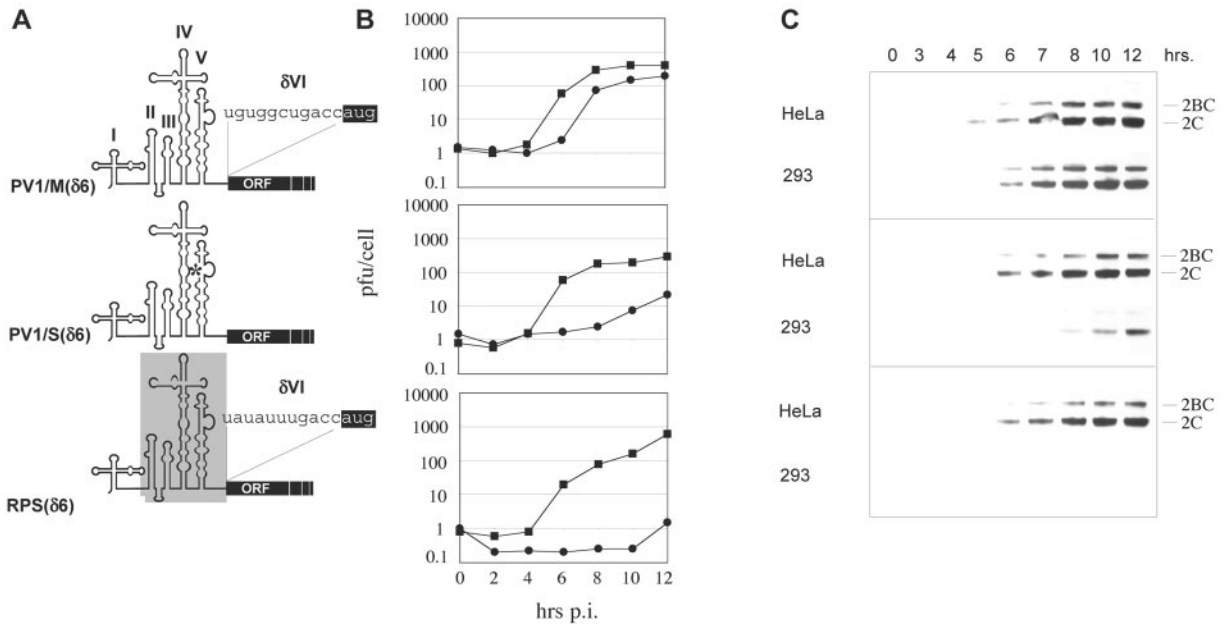

FIG. 3. Genetic structure (A), one-step growth curves (B), and viral gene expression (C) of PV1/M(δ6), PV1/S(δ6), and RPS(δ6). (A) The respective IRESes were manipulated by placing the conserved cryptic AUG codon (boxed black) in optimal Kozak context (. . .accAUGg. . .). This manipulation moved the translation initiation site upstream and deleted SLD VI. The sequence surrounding the artificial initiation codon of PV1/S(δ6) is identical to PV1/M(δ6). (B) One-step growth curves in HeLa (■) and HEK 293 (●) cells. (C) Viral gene expression was assessed by Western blot detection of the polioviral proteins 2C and 2BC at various hours p.i.

Given the evidence for a crucial role of SLD V in the attenuation phenotype of the Sabin strains, we focused our analyses of the genetic basis for neuronal function on the equivalent structure of the HRV2 IRES. We constructed RPS(δ6-PV5), which features an IRES composed of HRV2 SLD II-IV and PV1(M) SLD V (Fig. 4A). Propagation of this construct in HEK 293 cells was equivalent to PV1/M(δ6) (compare Fig. 3B with 5B), indicating that in the absence of SLD VI, PV1/M SLD V alone determines IRES activity in HEK 293 cells. Next, to fine-map the locus for neuronal IRES function, we generated a series of constructs where IRES SLD V was composed of mixed sequence derived of HRV2 and PV1(M) (Fig. 4B to D). Three recombinants based on RPS(δ6) [RPS(δ6-PV5a-c)] were engineered to contain chimeric SLD Vs featuring decreasing PV1(M) sequence content (Fig. 4B to D).

Virus propagation and gene expression rates of RPS(δ6-PV5a-c) in HeLa cells corresponded to those observed with RPS(δ6-PV5) (Fig. 5) and all other (δ6) constructs tested (compare to Fig. 3). In contrast, hybrid SLD V constructs exhibited variable performance in HEK 293 cells (Fig. 5B and C). Interestingly, the growth kinetics and gene expression profiles of the RPS(δ6-PV5a-c) constructs in HEK 293 cells revealed a gradual decline of neuronal IRES competence in step with decreasing PV1(M) sequence content (Fig. 5B and C). We observed a slightly delayed accumulation of viral progeny and gene products with RPS(δ6-PV5a) containing nt 483 to 519 of PV1(M) (Fig. 4B), which was exacerbated gradually with the RPS(δ6-PV5b) (Fig. 4C) and RPS(δ6-PV5c) (Fig. 4D) constructs. Even a marginal sequence divergence between RPS(δ6-PV5b) and RPS(δ6-PV5c) consisting of only 3 nt (compare Fig. 4C and D) conferred a slight replicative advantage in HEK 293 cells (Fig. 5B and C).

Our observations indicate that HRV2 SLD V as a whole, rather than through single residues, confers IRES incompetence in HEK 293 cells. These results implicate the secondary structure of HRV2 SLD V in neuronal IRES dysfunction. However, to claim that secondary structure alone is determining neuronal IRES incompetence would require the study of compensatory mutations. Our findings mirror earlier assumptions about the role of SLD V secondary structure in neuronal function of the Sabin IRESes (22, 34, 55) and point towards a common mechanism attenuating Sabin and HRV2 IRESes. Furthermore, HRV2 IRES neuronal incompetence based on structural features of an entire SLD, rather than a single deviant residue in the Sabin strains, would explain the more substantial neuronal deficit of the former. The more-solid genetic basis of neuroattenuation associated with the HRV2 IRES also suggests improved genetic stability of the attenuation phenotype over the Sabin strains.

Genetic stability profiles of RPS and PV1/S(IRES). The attenuation phenotype of PV recombinants replicating under control of the HRV2 IRES has proven to be stable upon passage in *CD155* transgenic mice and Sk-N-Mc neuroblastoma cells (19) as well as in malignant glioma cells (17). These findings are supported by the comparatively broad genetic basis for attenuation in the HRV2 IRES supplied by SLD V. However, since neuron-specific propagation deficits of RPS were substantially more pronounced in HEK 293 than in Sk-N-Mc neuroblastoma cells (Fig. 2), we reevaluated the stability of neuronal HRV2 and Sabin IRES dysfunction upon serial passage in this improved tissue culture model for PV neuronal replication profiles.

Serial passage of RPS in HEK 293 cells did not lead to the emergence of variants with enhanced cytopathogenic effect

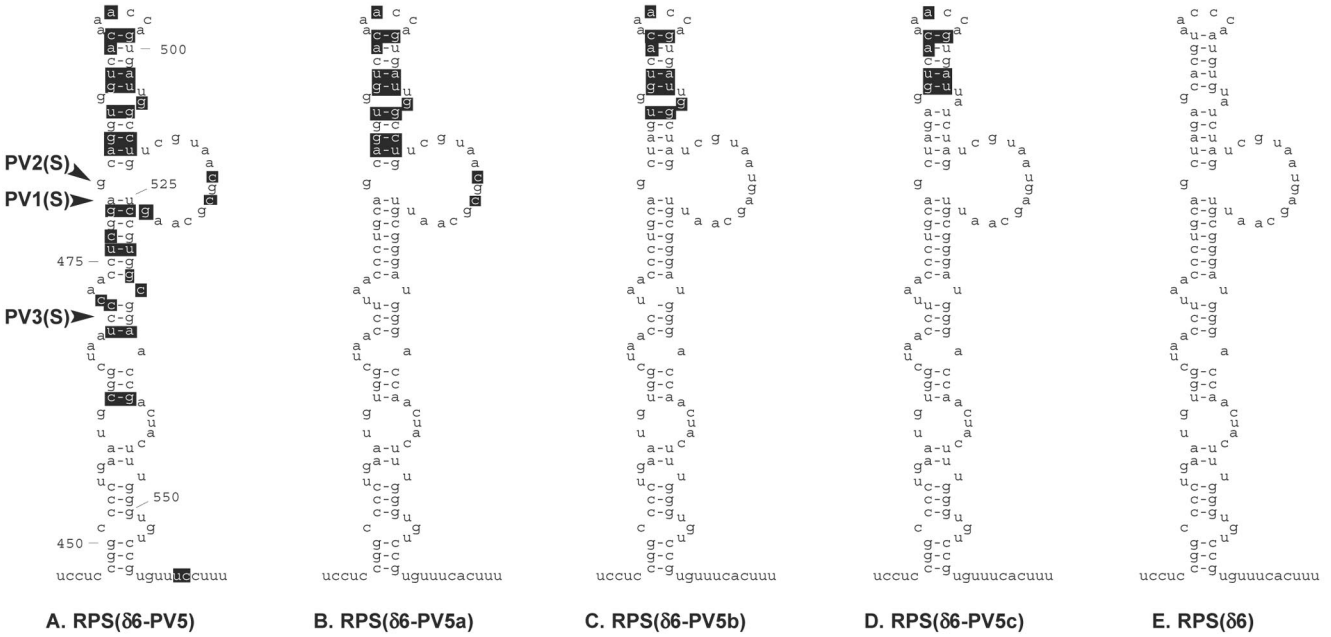

FIG. 4. Primary sequence and predicted secondary structure of the PV1(M), HRV2, and recombinant SLD Vs. Recombinant SLD Vs were inserted into the RPS(δ6) background, featuring HRV2 IRES SLD II-IV and deletion of SLD VI (see Materials and Methods). Nucleotides derived from PV sequence are shown in black boxes. (A) RPS(δ6-PV5) carries SLD V derived of PV1(M). Unboxed nucleotides are identical between HRV2 and PV1(M). The indicated positions of the attenuating mutations in the Sabin strains and the numbering refer to the sequence of PV1(M) (24). (B to D) RPS(δ6-PV5a-c) feature various sequence content derived of PV1(M) in the distal loop region of SLD V. (E) RPS(δ6) contains the HRV2 SLD V.

after 10 passages. Since, despite prolonged incubation periods, RPS barely propagates in HEK 293 cells (Fig. 2) serial passage leads to a gradual dilution of virus yield. Therefore, we did not recover sufficient progeny from the 10th passage of RPS in HEK 293 cells to conduct one-step growth curve and gene expression analyses. However, adequate yield of viral RNA allowed us to sequence reverse-transcribed viral genomic RNA isolated from the 10th passage in HEK 293 cells (see Materials and Methods). Comparison with sequence from the original inoculum revealed identical 5′ UTR sequences for input RPS and material recovered after 10 passages in HEK 293 cells.

In contrast, we observed improved growth capability of PV1/S(IRES) following serial passage in HEK 293 cells, which was evident after the fifth passage by the occurrence of characteristic cytopathic effects. Sequence analysis of reverse-transcribed RNA from the fifth passage revealed a mixture of viruses featuring either A (wt) or G [PV1(S)] at nt 480 (Fig. 6). Material recovered from the 10th passage no longer contained viral genetic material with the original PV1(S) IRES sequence but instead consistently featured the reversion of nt 480 (G→A) (Fig. 6).

Cell type-specific IRES function in a reporter context. Experiments assaying viral growth do not permit separation of IRES effects stemming from translation defects from those affecting RNA replication functions. To directly examine IRES translation, we designed subgenomic IRES-driven reporter constructs. pPV1(M)-Luc-PVA50 and pHRV-Luc-PVA50 feature a PV1(M) cloverleaf; the full-length PV1(M) and HRV2 IRES, respectively; a portion of the PV1(M) capsid protein coding sequence; the rLuc open reading frame; the PV1(M) 3′ UTR; and a 50-mer poly(A) tail (Fig. 7B). In vitro transcription of these constructs yielded reporter RNAs that were transfected into HeLa, Sk-N-Mc, and HEK 293 cells, along with a cap-driven reporter RNA containing the β-globin leader (Fig. 7A). We analyzed IRES and cap-dependent translation by measuring reporter expression at various intervals posttransfection.

Levels of IRES-driven translation were similar to cap-dependent translation in all three cell lines tested (Fig. 7C). Furthermore, PV1(M) and HRV2 IRES performance was roughly equivalent in both HeLa and HEK 293 cells (Fig. 7C). Unexpectedly, translation at the PV1(M) IRES was depressed in Sk-N-Mc cells compared to HRV2 IRES-directed translation (Fig. 7C). In contrast, HRV2 IRES-driven viral propagation of RPS is far inferior to PV containing its cognate IRES in these cells (Fig. 2). These results indicate that translation in a reporter context does not recapitulate the neuron-specific functional deficit of the HRV2 IRES in the context of the PV genome.

DISCUSSION

The emergence of epidemic poliomyelitis in the 20th century fueled intense efforts to determine the basis for PV's propensity to cause paralysis. Researchers quickly realized that the intrinsic neuropathogenic potential of PV field isolates varies considerably (reviewed in reference 4), a finding that inspired the selection for viral isolates with deficient CNS propagation phenotypes (48). Historically, PV neuroattenuation has been assessed in nonhuman primates but, recently, mice transgenic

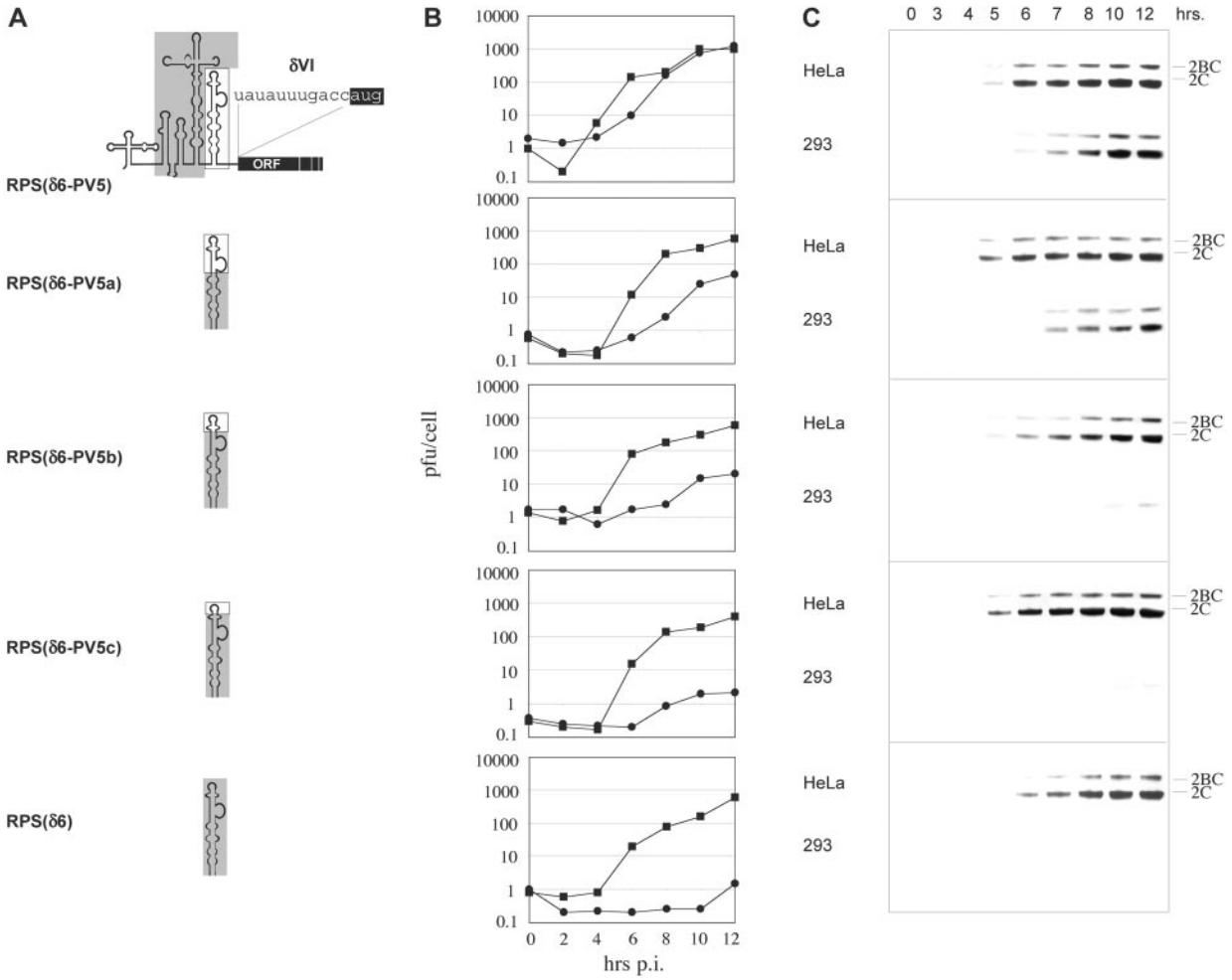

FIG. 5. Genetic structure (A), viral propagation (B), and gene expression (C) of RPS derivatives carrying SLD Vs shown in Fig. 4. (A) The composition of SLD V for the respective constructs is schematically indicated. Refer to Fig. 4 for detailed sequence information. (B and C) Replication profile and time course of viral gene expression in HeLa (■) and HEK 293 (●) cells.

for the human PV receptor have emerged as a viable alternative (11). Experimental animal models, although indispensable for evaluation of neuropathogenicity in vivo, are difficult to use in routine studies in the laboratory. Furthermore, separate assessment of facets of the neurovirulent phenotype, e.g., the effect of IRES structure on neuronal translation, is problematic in animals, where a myriad of viral and host-related factors influence pathogenicity.

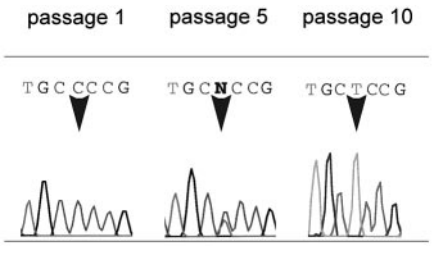

FIG. 6. Emergence of wt PV1(M) IRES sequence upon serial passage of PV1/S(IRES) in HEK 293 cells. The arrows indicate the position of nt 480 in SLD V of the PV1(S) IRES. The 5th passage contained mixed populations (G→A/G), while after 10 passages only the wt IRES (G→A) was detected. Sequence was generated using a 3′ primer and thus reads 3′ to 5′.

Agol et al. (1) and LaMonica and Racaniello (32) first reported the Sabin attenuation phenotype to extend to human neuroblastoma cell lines, thus providing a tissue culture model for the study of PV neurovirulence. However, most neuroblastoma cell lines have serious shortcomings as neuronal model systems. They are heterogeneous cancer cell populations of uncertain origin capable of spontaneous interconversion between a neuroblast- and fibroblast-like morphology (47). The latter is associated with reduced neuritic process extension, neurotransmitter synthesis, and neuronal surface marker expression (46).

Our comparative analyses of viral growth and gene expression phenotypes of PV1(M), PV1(S), and RPS revealed that HEK 293 cells recapitulate the neuron-specific functional deficits of the Sabin and HRV2 IRESes previously established in neuroblastoma cells (1, 19, 32), CD155 transgenic mice (19, 45), and nonhuman primates (18, 48). The attenuation pheno-

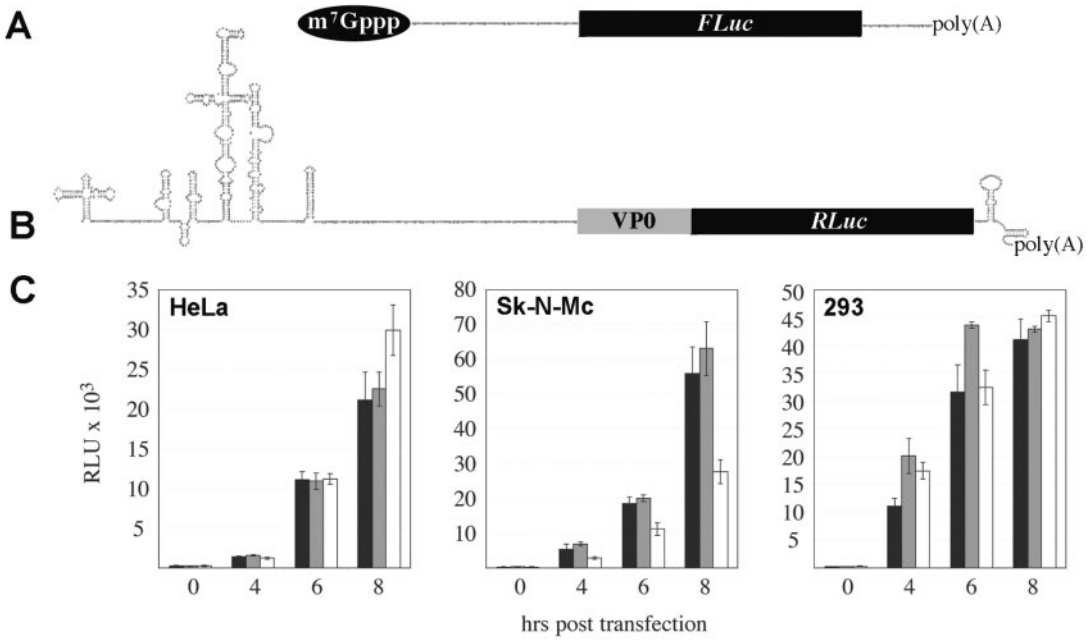

FIG. 7. Translation of IRES reporter RNAs in HeLa, Sk-N-Mc, and HEK 293 cells. Capped RNA transcripts expressing fLuc under control of the β-globin leader (A) or uncapped IRES-controlled RNAs (B) were transfected into cells. (C) Translation of the capped control (black bars) and reporter constructs containing the HRV2 (grey bars) or PV1(M) IRES (white bars) was evaluated at several intervals posttransfection as described in Materials and Methods. The values are averages of triplicate samples, and the error bars indicate standard deviation.

type of both PV1(S) and RPS, determined by the propagation differentials in HeLa versus HEK 293 cells relative to PV1(M), was far more pronounced in HEK 293 than in Sk-N-Mc neuroblastoma cells.

Our observations confirm previous reports casting doubt on the classification of HEK 293 cells as kidney tubular epithelial and stress the possibility that they are of neuroblastic origin (50). Furthermore, Western blot analyses of HEK 293 lysates demonstrate intermediate filament expression commensurate with neuronal origin. However, classification of cultured cell lines according to expression patterns of selected markers must be approached with caution. This is aptly illustrated by DMS79, a small cell lung cancer cell line, which expresses an array of conventional neuronal markers (Fig. 1) but is fully susceptible to the highly neuroattenuated RPS (data not shown). At this stage, the classification of HEK 293 cells cannot be considered definite, and an unambiguous correlation of cell differentiation markers with pathogenic PV phenotypes may remain difficult. However, we have accumulated convincing evidence that PV replication in HEK 293 cells recapitulates the attenuation phenotype and its genetic determinants previously described in neuroblastoma cells and experimental animals. HEK 293 may become a valuable resource for studies of PV neurovirulence and its molecular determinants in a convenient cell culture system superior to cancerous cell lines of dubious or fluctuating identity.

Our observations suggest a common genetic basis for neuroattenuation mediated by Sabin- and HRV2 IRESes. In both structures, the distal stem of IRES SLD V critically influences neuronal viral gene expression and particle propagation, most likely due to secondary structure formation interfering with efficient IRES function (22, 35, 51). This scenario suggests involvement of RNA-binding proteins with affinity for IRES secondary structural features. Neuronal IRES incompetence could be caused by cell- or organ-specific distribution or activity of such proteins. A number of IRES *trans*-acting factors, including the polypyrimidine tract binding protein (PTB) (24), poly(rC)-binding protein (57), and upstream of N-ras (unr) (25), have been reported to interact with the HRV2 IRES. Of these, PTB and its neuronal isoform nPTB or brPTB (36) have been reported to influence picornavirus IRES function in a cell type-specific manner (44). We recently found that the double-stranded RNA binding protein 76, isolated from cytoplasmic extracts of neuronal cells, interacts with HRV2 IRES SLD. V/VI and inhibits HRV IRES-driven translation in cells of neuronal lineage (M. K. Merrill and M. Gromeier, submitted for publication). IRES *trans*-acting factors with cell type-specific distribution may affect translation stimulation through their effects on template closure, since neuronal HRV2 IRES function has been linked to structures within the 3′ UTR (9).

Traditionally, the IRES has been implicated in the control of viral gene expression, but Borman et al. reported involvement of SLD V in PV genome replication (5). Although recent evidence from the study of subgenomic PV replicons reached contrary conclusions (37), a regulatory role of IRES sequence in genome replication cannot be excluded. PV protein synthesis and genome replication are intertwined processes that are both reported to involve genome end-to-end communication (2, 3, 23, 54). It is thus reasonable to assume that influences on translation and RNA replication at the same circular template may overlap. Observations implicating IRES-3′ UTR communication in neuron-specific PV growth (9) support the genome closure model and a possible role for the IRES in RNA replication functions (recently discussed in reference 49).

Our experiments with reporter RNAs suggest that IRES-mediated propagation deficits in neuronal cells cannot be explained by translation competence of the IRES itself. We found equivalent HRV2 IRES performance in cells permissive and nonpermissive for PVS-RIPO propagation. It should be born in mind, however, that IRES function is optimized by virus-induced modifications of the translation apparatus, which dramatically change the conditions for protein synthesis. Assays with IRESes outside the context of the viral genome do not recapitulate these conditions. We speculate that viral gene products and their effects on host cells in different tissues may contribute to the influence of IRES on PV pathogenesis.

Despite enormous success in the PV eradication campaign, complications have arisen from use of the Sabin vaccine strains. These strains can rapidly revert to a neurovirulent phenotype (which usually involves reversion to the wt IRES SLD V sequence) in infected cultured cells (7), normal human vaccinees (20), and patients with VAPP. Indeed, we observed rapid reversion of PV1(S) at nt 480 upon passage in HEK 293 cells. The traditional view that vaccine revertants lack the ability to initiate circulation (62) has been challenged by a string of poliomyelitis outbreaks in Hispaniola, Egypt, Madagascar, and the Philippines (discussed in reference 6) that were attributed to circulating vaccine variants. The comparatively weak neuron-specific IRES deficit associated with PV1(S) nt 480 and its rapid reversion upon passage in culture underscore prior observations of a "blurred line" separating attenuated from neurovirulent PV strains (6). Our studies suggest very favorable attenuation and genetic stability profiles for PVs replicating under control of the HRV2 IRES, manifest through persistently repressed propagation and gene expression in cells of neuronal lineage.

Combining the favorable features of the HRV2 IRES with the PV1(S) capsid attenuation determinants (RPS) has produced a live attenuated poliovirus variant whose attenuation level and genetic stability profile in vitro far exceed that of PV1(S). Although experience with mass vaccination of human populations is absent, prototype engineered highly attenuated PVs with heterologous HRV2 IRES elements may provide safer alternatives to existing live attenuated vaccine strains.

ACKNOWLEDGMENTS

We thank M. Burdick and M. Merrill for reagents and technical advice and S. Bradrick for critical review.

This work was supported by Public Health Service grants CA87537 (M.G.) and AI054216 (M.G.). S.A.C. is supported by a Susan G. Komen Breast Cancer Foundation Dissertation Research Award. M.G. is a recipient of a Burroughs Wellcome Career Award in the Biomedical Sciences.

REFERENCES

1. **Agol, V. I., S. G. Drozdov, T. A. Ivannikova, M. S. Kolesnikova, M. B. Korolev, and E. A. Tolskaya.** 1989. Restricted growth of attenuated poliovirus strains in cultured cells of a human neuroblastoma. J. Virol. **63:**4034–4038.
2. **Barton, D. J., B. J. O'Donnell, and J. B. Flanegan.** 2001. 5′ cloverleaf in poliovirus RNA is a *cis*-acting replication element required for negative-strand synthesis. EMBO J. **20:**1439–1448.
3. **Bergamini, G., T. Preiss, and M. W. Hentze.** 2000. Picornavirus IRESes and the poly(A) tail jointly promote cap-independent translation in a mammalian cell-free system. RNA **6:**1781–1790.
4. **Bodian, D.** 1972. Poliomyelitis, p. 2323–2343. *In* J. Minckler (ed.), Pathology of the nervous system. McGraw-Hill, New York, N.Y.
5. **Borman, A. M., F. G. Deliat, and K. M. Kean.** 1994. Sequences within the poliovirus internal ribosome entry segment control viral RNA synthesis. EMBO J. **13:**3149–3157.
6. **Cherkasova, E., M. Laassri, V. Chizhikov, E. Korotkova, E. Dragunsky, V. I. Agol, and K. Chumakov.** 2003. Microarray analysis of evolution of RNA viruses: evidence of circulation of virulent highly divergent vaccine-derived polioviruses. Proc. Natl. Acad. Sci. USA **100:**9398–9403.
7. **Chezzi, C., C. J. Dommann, N. K. Blackburn, E. Maselesele, J. McAnerney, and B. D. Schoub.** 1998. Genetic stability of oral polio vaccine prepared on primary monkey kidney cells or Vero cells—effects of passage in cell culture and the human gastrointestinal tract. Vaccine **16:**2031–2038.
8. **Christodoulou, C., F. Colbere-Garapin, A. Macadam, L. F. Taffs, S. Marsden, P. Minor, and F. Horaud.** 1990. Mapping of mutations associated with neurovirulence in monkeys infected with Sabin 1 poliovirus revertants selected at high temperature. J. Virol. **64:**4922–4929.
9. **Dobrikova, E., P. Florez, S. Bradrick, and M. Gromeier.** 2003. Activity of a type 1 picornavirus internal ribosomal entry site is determined by sequences within the 3′ non-translated region. Proc. Natl. Acad. Sci. USA **100:**15125–15130.
10. **Dobrikova, E. Y., P. Florez, and M. Gromeier.** 2003. Structural determinants of insert retention of poliovirus expression vectors with recombinant IRES elements. Virology **311:**241–253.
11. **Dragunsky, E., T. Nomura, K. Karpinski, J. Furesz, D. J. Wood, Y. Pervikov, S. Abe, T. Kurata, O. Vanloocke, G. Karganova, R. Taffs, A. Heath, A. Ivshina, and I. Levenbook.** 2003. Transgenic mice as an alternative to monkeys for neurovirulence testing of live oral poliovirus vaccine: validation by a W.H.O. collaborative study. Bull. W. H. O. **81:**251–260.
12. **Dufresne, A. T., E. Y. Dobrikova, S. Schmidt, and M. Gromeier.** 2002. Genetically stable picornavirus expression vectors with recombinant internal ribosomal entry sites. J. Virol. **76:**8966–8972.
13. **Evans, D. M. A., G. Dunn, P. D. Minor, G. C. Schild, A. J. Cann, G. Stanway, J. W. Almond, K. Currey, and J. V. Maizel.** 1985. Increased neurovirulence associated with a single nucleotide change in a noncoding region of the Sabin type 3 poliovaccine genome. Nature **314:**548–550.
14. **Gmyl, A. P., E. V. Pilipenko, S. V. Maslova, G. A. Belov, and V. I. Agol.** 1993. Functional and genetic plasticities of the poliovirus genome: quasi-infectious RNAs modified in the 5′-untranslated region yield a variety of pseudorevertants. J. Virol. **67:**6309–6316.
15. **Graham, F. L., J. Smiley, W. C. Russell, and R. Nairn.** 1977. Characteristics of a human cell line transformed by DNA from human adenovirus type 5. J. Gen. Virol. **36:**59–74.
16. **Gromeier, M., and A. Nomoto.** 2002. Determinants of poliovirus pathogenesis, p. 367–379. *In* B. Semler and E. Wimmer (ed.), Molecular biology of picornaviruses. ASM Press, Washington, D.C.
17. **Gromeier, M., S. Lachmann, M. Rosenfeld, P. H. Gutin, and E. Wimmer.** 2000. Intergeneric poliovirus recombinants for the treatment of malignant glioma. Proc. Natl. Acad. Sci. USA **97:**6803–6808.
18. **Gromeier, M., B. Bossert, M. Arita, A. Nomoto, and E. Wimmer.** 1999. Dual stem loops within the poliovirus internal ribosomal entry site control neurovirulence. J. Virol. **73:**958–964.
19. **Gromeier, M., L. Alexander, and E. Wimmer.** 1996. Internal ribosomal entry site substitution eliminates neurovirulence in intergeneric poliovirus recombinants. Proc. Natl. Acad. Sci. USA **93:**2370–2375.
20. **Guillot, S., D. Otelea, F. Delpeyroux, and R. Crainic.** 1994. Point mutations involved in the attenuation/neurovirulence alternation in type 1 and 2 oral polio vaccine strains detected by site-specific polymerase chain reaction. Vaccine **12:**503–507.
21. **Haller, A. A., S. R. Stewart, and B. L. Semler.** 1996. Attenuation stem-loop lesions in the 5′ noncoding region of poliovirus RNA: neuronal cell-specific translation defects. J. Virol. **70:**1467–1474.
22. **Haller, A. A., and B. L. Semler.** 1995. Stem-loop structure synergy in binding cellular proteins to the 5′ noncoding region of poliovirus RNA. Virology **206:**923–934.
23. **Herold, J., and R. Andino.** 2001. Poliovirus RNA replication requires genome circularization through a protein-protein bridge. Mol. Cell **7:**581–591.
24. **Hunt, S. L., and R. J. Jackson.** 1999. Polypyrimidine-tract binding protein (PTB) is necessary, but not sufficient, for efficient internal initiation of translation of human rhinovirus-2 RNA. RNA **5:**344–359.
25. **Hunt, S. L., J. J. Hsuan, N. Totty, and R. J. Jackson.** 1999. Unr, a cellular cytoplasmic RNA-binding protein with five cold-shock domains, is required for internal initiation of translation of human rhinovirus RNA. Genes Dev. **13:**437–448.
26. **Iizuka, N., M. Kohara, K. Hagino-Yamagishi, S. Abe, T. Komatsu, K. Tago, M. Arita, and A. Nomoto.** 1989. Construction of less neurovirulent polioviruses by introducing deletions into the 5′ noncoding sequence of the genome. J. Virol. **63:**5354–5363.
27. **Jang, S. K., H. G. Kräusslich, M. J. H. Nicklin, G. M. Duke, A. C. Palmenberg, and E. Wimmer.** 1988. A segment of the 5′ nontranslated region of encephalomyocarditis virus RNA directs internal entry of ribosomes during in vitro translation. J. Virol. **62:**2636–2643.
28. **Katsetos, C. D., M. M. Herman, and S. J. Mork.** 2003. Class III beta-tubulin in human development and cancer. Cell Motil. Cytoskelet. **55:**77–96.
29. **Kawamura, N., M. Kohara, S. Abe, T. Komats, K. Tago, M. Arita, and A.**

Nomoto. 1989. Determinants in the 5′ noncoding region of poliovirus Sabin 1 RNA that influence the attenuation phenotype. J. Virol. **63:**1302–1309.
30. **Kitamura, N., B. L. Semler, P. G. Rothberg, G. R. Larsen, C. J. Adler, A. J. Dorner, E. A. Emini, R. Hanecak, J. J. Lee, S. van der Werf, C. W. Anderson, and E. Wimmer.** 1981. Primary structure, gene organization and polypeptide expression of poliovirus RNA. Nature **291:**547–553.
31. **Kuge, S., and A. Nomoto.** 1987. Construction of viable deletion and insertion mutants of the Sabin strain of type 1 poliovirus: function of the 5′ noncoding sequence in viral replication. J. Virol. **61:**1478–1487.
32. **La Monica, N., and V. R. Racaniello.** 1989. Differences in replication of attenuated and neurovirulent polioviruses in human neuroblastoma cell line SH-SY5Y. J. Virol. **63:**2357–2360.
33. **Lee, M. K., and D. W. Cleveland.** 1996. Neuronal intermediate filaments. Annu. Rev. Neurosci. **19:**187–217.
34. **Macadam, A. J., S. R. Pollard, G. Ferguson, R. Skuce, D. Wood, J. W. Almond, and P. D. Minor.** 1993. Genetic basis of attenuation of the Sabin type 2 vaccine strain of poliovirus in primates. Virology **192:**18–26.
35. **Macadam, A. J., G. Ferguson, J. Burlison, D. Stone, R. Skuce, J. W. Almond, and P. D. Minor.** 1992. Correlation of RNA secondary structure and attenuation of Sabin vaccine strains of poliovirus in tissue culture. Virology **189:**415–422.
36. **Markovtsov, V., J. M. Nikolic, J. A. Goldman, C. W. Turck, M. Y. Chou, and D. L. Black.** 2000. Cooperative assembly of an hnRNP complex induced by a tissue-specific homolog of polypyrimidine tract binding protein. Mol. Cell. Biol. **20:**7463–7479.
37. **Murray, K. E., B. P. Steil, A. W. Roberts, and D. J. Barton.** 2004. Replication of poliovirus RNA with complete internal ribosome entry site deletions. J. Virol. **78:**1393–1402.
38. **Nomoto, A., T. Omata, H. Toyoda, S. Kuge, H. Horie, Y. Kataoka, Y. Genba, Y. Nakano, and N. Imura.** 1982. Complete nucleotide sequence of the attenuated poliovirus Sabin 1 strain genome. Proc. Natl. Acad. Sci. USA **79:**5793–5797.
39. **Ochs, K., A. Zeller, L. Saleh, G. Bassili, Y. Song, A. Sonntag, and M. Niepmann.** 2003. Impaired binding of standard initiation factors mediates poliovirus translation attenuation. J. Virol. **77:**115–122.
40. **Ohka, S., and A. Nomoto.** 2001. The molecular basis of poliovirus neurovirulence. Dev. Biol. **105:**51–58.
41. **Paul, A. V., J. Mugavero, J. Yin, S. Hobson, S. Schultz, J. H. van Boom, and E. Wimmer.** 2000. Studies on the attenuation phenotype of polio vaccines: poliovirus RNA polymerase derived from Sabin type 1 sequence is temperature sensitive in the uridylylation of VPg. Virology **272:**72–84.
42. **Pelletier, J., and N. Sonenberg.** 1988. Internal initiation of translation of eukaryotic mRNA directed by a sequence derived from poliovirus RNA. Nature **334:**320–325.
43. **Pilipenko, E. V., A. P. Gmyl, S. V. Maslova, Y. V. Svitkin, A. N. Sinyakov, and V. I. Agol.** 1992. Prokaryotic-like *cis* elements in the cap-independent internal initiation of translation on picornavirus RNA. Cell **68:**119–131.
44. **Pilipenko, E. V., E. G. Viktorova, S. T. Guest, V. I. Agol, and R. P. Roos.** 2001. Cell-specific proteins regulate viral RNA translation and virus-induced disease. EMBO J. **20:**6899–6908.
45. **Ren, R. B., F. Costantini, E. J. Gorgacz, J. J. Lee, and V. R. Racaniello.** 1990. Transgenic mice expressing a human poliovirus receptor: a new model for poliomyelitis. Cell **63:**353–362.
46. **Rettig, W. J., B. A. Spengler, P. G. Chesa, L. J. Old, and J. L. Biedler.** 1987. Coordinate changes in neuronal phenotype and surface antigen expression in human neuroblastoma cell variants. Cancer Res. **47:**1383–1389.
47. **Ross, R. A., B. A. Spengler, and J. L. Biedler.** 1983. Coordinate morphological and biochemical interconversion of human neuroblastoma cells. J. Nat. Cancer Inst. **71:**741–749.
48. **Sabin, A. B.** 1965. Oral poliovirus vaccine. History of its development and prospects for eradication of poliomyelitis. JAMA **194:**872–876.
49. **Semler, B.** 2004. Poliovirus proves IRES-istible in vivo. J. Clin. Investig. **113:**1678–1681.
50. **Shaw, G., S. Morse, M. Ararat, and F. L. Graham.** 2002. Preferential transformation of human neuronal cells by human adenoviruses and the origin of HEK 293 cells. FASEB J. **16:**869–871.
51. **Skinner, M. A., V. R. Racaniello, G. Dunn, J. Cooper, P. D. Minor, and J. W. Almond.** 1989. New model for the secondary structure of the 5′ non-coding RNA of poliovirus is supported by biochemical and genetic data that also show that RNA secondary structure is important in neurovirulence. J. Mol. Biol. **207:**379–392.
52. **Stanway, G., P. J. Hughes, R. C. Mountford, P. Reeve, P. D. Minor, G. C. Schild, and J. W. Almond.** 1984. Comparison of the complete nucleotide sequences of the genomes of the neurovirulent poliovirus P3/Leon/37 and its attenuated Sabin vaccine derivative P3/Leon 12a1b. Proc. Natl. Acad. Sci. USA **81:**1539–1543.
53. **Stanway, G., A. J. Cann, R. Hauptmann, P. Hughes, L. D. Clarke, R. C. Mountford, P. D. Minor, G. C. Schild, and J. W. Almond.** 1983. The nucleotide sequence of poliovirus type 3 Leon 12 a1b: comparison with poliovirus type 1. Nucleic Acids Res. **11:**5629–5643.
54. **Svitkin, Y. V., H. Imataka, K. Khaleghpour, A. Kahvejian, H. D. Liebig, and N. Sonenberg.** 2001. Poly(A)-binding protein interaction with elF4G stimulates picornavirus IRES-dependent translation. RNA **7:**1743–1752.
55. **Svitkin, Y. V., N. Cammack, P. D. Minor, and J. W. Almond.** 1990. Translation deficiency of the Sabin type 3 poliovirus genome: association with an attenuating mutation C472→U. Virology **175:**103–109.
56. **Toyoda, H., M. Kohara, Y. Kataoka, T. Suganuma, T. Omata, N. Imura, and A. Nomoto.** 1984. Complete nucleotide sequences of all three poliovirus serotype genomes. Implication for genetic relationship, gene function and antigenic determinants. J. Mol. Biol. **174:**561–585.
57. **Walter, B. L., J. H. Nguyen, E. Ehrenfeld, and B. Semler.** 1999. Differential utilization of poly(rC) binding protein 2 in translation directed by picornavirus IRES elements. RNA **5:**1570–1585.
58. **Weeks-Levy, C., J. M. Tatem, S. J. DiMichele, W. Waterfield, A. F. Georgiu, and S. J. Mento.** 1991. Identification and characterization of a new base substitution in the vaccine strain of Sabin 3 poliovirus. Virology **185:**934–937.
59. **Westrop, G. D., K. A. Wareham, D. M. Evans, G. Dunn, P. D. Minor, D. I. Magrath, F. Taffs, S. Marsden, M. A. Skinner, G. C. Schild, and J. W. Almond.** 1989. Genetic basis of attenuation of the Sabin type 3 oral poliovirus vaccine. J. Virol. **63:**1338–1344.
60. **W.H.O. Collaborative Study Group.** 1982. The relationship between persisting spinal paralysis and poliomyelitis vaccine—results of a ten-year inquiry. Bull. W. H. O. **60:**231–242.
61. **Wimmer, E., C. U. T. Hellen, and X. Cao.** 1983. Genetics of poliovirus. Annu. Rev. Genet. **27:**353–436.
62. **Wood, D. J., R. W. Sutter, and W. R. Dowdle.** 2000. Stopping poliovirus vaccination after eradication: issues and challenges. Bull. W. H. O. **78:**347–357.